Regular Article – Hadron Physics

Study of ω-meson production in pp collisions at ANKE

S. Barsov[1], M. Büscher[2], M. Hartmann[2], V. Hejny[2], A. Kacharava[3,4], I. Keshelashvili[2,4], A. Khoukaz[5],
V. Koptev[1], P. Kulessa[6], A. Kulikov[7], I. Lehmann[8], V. Leontyev[2], G. Macharashvili[4,7], Y. Maeda[9], T. Mersmann[5],
S. Merzliakov[2,7], S. Mikirtychyants[1], A. Mussgiller[3], D. Oellers[2], H. Ohm[2], F. Rathmann[2], R. Schleichert[2,a],
H. Seyfarth[2,b], H. Ströher[2], S. Trusov[10,11], Yu. Valdau[2,1], P. Wüstner[12], S. Yaschenko[3,7], and C. Wilkin[13]

[1] High Energy Physics Department, Petersburg Nuclear Physics Institute, 188350 Gatchina, Russia
[2] Institut für Kernphysik, Forschungszentrum Jülich, D-52425 Jülich, Germany
[3] Physikalisches Institut II, Universität Erlangen-Nürnberg, 91058 Erlangen, Germany
[4] High Energy Physics Institute, Tbilisi State University, 0186 Tbilisi, Georgia
[5] Institut für Kernphysik, Universität Münster, 48149 Münster, Germany
[6] Institute of Nuclear Physics, 31342 Cracow, Poland
[7] Laboratory of Nuclear Problems, Joint Institute for Nuclear Research, 141980 Dubna, Russia
[8] Physics and Astronomy Department, University of Glasgow, Glasgow G12 8QQ, UK
[9] Research Center for Nuclear Physics, Osaka University, Ibaraki, 567-0047 Osaka, Japan
[10] Institut für Kern- und Hadronenphysik, Forschungszentrum Rossendorf, 01314 Dresden, Germany
[11] Lomonosov Moscow State University Skobeltsyn Institute of Nuclear Physics, 119992 Moscow, Russia
[12] Zentralinstitut für Elektronik, Forschungszentrum Jülich, 52425 Jülich, Germany
[13] Physics and Astronomy Department, UCL, London, WC1E 6BT, UK

Abstract. The production of ω-mesons in the $pp \to pp\omega$ reaction has been investigated with the COSY-ANKE spectrometer for excess energies of 60 and 92 MeV by detecting the two final protons and reconstructing their missing mass. The large physical background was subtracted using an event-by-event transformation of the proton momenta between the two energies. Differential distributions and total cross-sections were obtained after careful studies of possible systematic uncertainties in the overall ANKE acceptance. The results are compared with the predictions of theoretical models. Combined with data on the ϕ-meson, a more refined estimate is made of the Okubo-Zweig-Iizuka rule violation in the ϕ/ω production ratio.

PACS. 13.75.-n Hadron-induced low- and intermediate-energy reactions and scattering (energy ≤ 10 GeV) – 13.60.Le Meson production – 14.40.Cs Other mesons with $S = C = 0$, mass < 2.5 GeV

1 Introduction

The nucleon-nucleon system is strongly coupled to channels that contain one or multiple mesons. The production of these in NN collisions, preferably near their respective thresholds, will test and constrain theoretical models since, in these cases, only few partial waves contribute. The production of pions and heavier pseudoscalar mesons including kaons has been systematically studied in proton-proton interactions in the near-threshold region [1]. Now vector mesons, such as ρ and ω, are significant contributors to the NN force at short distances but for these

particles much less information is available on their production mechanism due to the lack of experimental data. The relative production of the isoscalar ω- and ϕ-mesons has recently received renewed interest in connection with the so-called Okubo-Zweig-Iizuka (OZI) rule [2]. This ratio may give information on the admixture of strange quarks in the nucleon only if the production mechanism is known to be the same for both mesons [3–5]. The conditions can be best controlled through near-threshold measurements but, as yet, the experimental data set is rather limited.

In the ω case, the $pp \to pp\omega$ total cross-section was measured for excess energies $Q \le 30$ MeV at SATURNE by detecting the two protons in the SPESIII magnetic spectrometer and identifying the meson by the missing-mass method [6]. In a more exclusive experiment, the DISTO Collaboration also measured ω production but at

much higher energy ($Q \approx 320\,\mathrm{MeV}$) [7]. The only data between these two energies were taken at COSY-TOF, a non-magnetic time-of-flight spectrometer, where the reaction was studied at $Q = 92$ and $173\,\mathrm{MeV}$ [8]. This latter energy is in fact the lowest for which differential distributions are available. Extra data are therefore required to fill the gap and establish the energy dependence of the total cross-section. For this purpose we here present ω results obtained using the COSY-ANKE facility at 60 and $92\,\mathrm{MeV}$. It is relevant within the OZI context to note that the DISTO group measured ϕ production at $82\,\mathrm{MeV}$, and we have recently published similar data at 18.5, 34.5, and $75.9\,\mathrm{MeV}$ [9].

The experimental facility at our disposal is described in sect. 2, where particle identification and efficiency determination, as well as the extraction of the luminosity, are also discussed. Since the ω-meson production is identified from the missing mass of two final protons, one of the major problems is a large physical background under the ω peak. We use the same kinematic transformation as proposed in the SPESIII analysis to estimate this background by employing data obtained at the other energy. This is the crucial element of the $pp \to pp\omega$ event selection, which is treated in detail in sect. 3. The acceptance for the two protons from the $pp \to pp\omega$ reaction available in this experiment was far from complete. Acceptance corrections could therefore only be done in a model-dependent way. For this purpose, various one-dimensional differential distributions were obtained and compared in sect. 4 with the results of simulations based on different model assumptions. The values of the total cross-sections given in sect. 5 are compared with the results of several theoretical approaches. Also to be found there is a discussion of how our data influence the extraction of the OZI ratio from near-threshold ω/ϕ production. Our conclusions and thoughts for future investigations are presented in sect. 6.

2 Experimental set-up and raw data analysis

The measurement has been carried out at the ANKE installation [10], using the internal hydrogen cluster-jet target [11] and COSY circulating proton beam. To reduce systematic effects, the beam momentum was changed every 10 minutes between $2.85\,\mathrm{GeV}/c$ and $2.95\,\mathrm{GeV}/c$, corresponding to excess energies of $60\,\mathrm{MeV}$ and $92\,\mathrm{MeV}$, respectively. Charged particles resulting from beam-target interactions, and going forward with laboratory polar angles up to $20°$, were deflected by the central dipole D2 onto the ANKE detector systems. In the present investigation, one final proton was detected in the ANKE forward detector (FD), passing through a set of three multiwire proportional chambers (MWPCs) and two layers of scintillators placed downstream of D2 and close to the beam pipe. The other proton was detected in coincidence in the positive charge detector system (PD), positioned to the right of D2. This system includes one layer of 23 thin start scintillators (SA) placed close to the exit window of the D2 vacuum chamber, two MWPCs, and one layer of six large stop scintillators (SW) within the ANKE Side Wall.

Only that part of the PD which has acceptance for the $pp \to pp\omega$ reaction was used in this experiment.

The chosen trigger of the coincidence of signals from the FD and SW scintillators did not permit the detection of proton-proton elastic scattering due to the kinematics of this reaction. Therefore, 1% of the count rate from the FD scintillators alone was added to the trigger stream so that the data could be normalised. The momenta of these particles were reconstructed and pp elastic scattering identified from the clear peak in the missing-mass distribution at the nominal proton mass. The data were corrected for the efficiency of the FD MWPCs on an event-by-event basis, as described below. Since the elastic-scattering peak had a width of $80\,\mathrm{MeV}/c^2$ FWHM, it was quite well separated from the inelastic continuum, which starts to be sizeable only above $1.08\,\mathrm{GeV}/c^2$. The ratio of the bin content at $1.05\,\mathrm{GeV}/c^2$ to that at the maximum of the proton peak was only about 2% and the contribution of the background under the peak is estimated to be $(1.8 \pm 0.8)\%$. The number of protons elastically scattered between laboratory angles of $6.6°$ and $8.8°$ was then determined from a fit of the peak by a Gaussian, with a polynomial background. Using predictions for the differential cross-section from the SAID database [12], the same average luminosity of $7.5 \times 10^{30}\,\mathrm{cm}^{-2}\,\mathrm{s}^{-1}$ was found for the two incident momenta, the values being constant over the angular range to better than 2%. The corresponding integral luminosities were $0.280\,\mathrm{pb}^{-1}$ and $0.273\,\mathrm{pb}^{-1}$ at $2.85\,\mathrm{GeV}/c$ and $2.95\,\mathrm{GeV}/c$, respectively. The overall systematic error of about 6% was estimated taking into account the uncertainty in the SAID calibration standard ($\sim 5\%$), the efficiency determination ($\sim 1\%$), and the $0.1°$ precision in the determination of the scattering angle ($\sim 3\%$).

As the $pp \to pp\omega$ reaction has to be identified from the missing mass with respect to the two protons, these were distinguished from other particles, mostly pions, using the time-of-flight (TOF) technique and momentum determination.

Although the SW scintillators are capable of delivering a momentum acceptance of the PD up to $1.6\,\mathrm{GeV}/c$, in the actual configuration of the equipment the momentum range had to be limited to be below $1.1\,\mathrm{GeV}/c$. Under these conditions, the time of flight between SA and SW scintillators alone provided sufficient particle identification. As an example of this, fig. 1 represents the TOF spectrum corresponding to the worst case of pion-proton separation.

The total efficiency of the momentum reconstruction in the PD could be determined for each of the SA-SW combinations because both of the MWPCs are placed between these scintillators. It was ensured that all of the typically $(15\text{--}25) \times 10^4$ protons detected in each of the SA-SW combinations passed through sensitive areas of both of the MWPCs. The numbers of protons before and after the reconstruction of their momenta were extracted from the corresponding TOF spectrum, which is similar to the one presented in fig. 1. The accidental background was significantly suppressed by the requirement to have some particle track reconstructed in the FD. The efficiency was
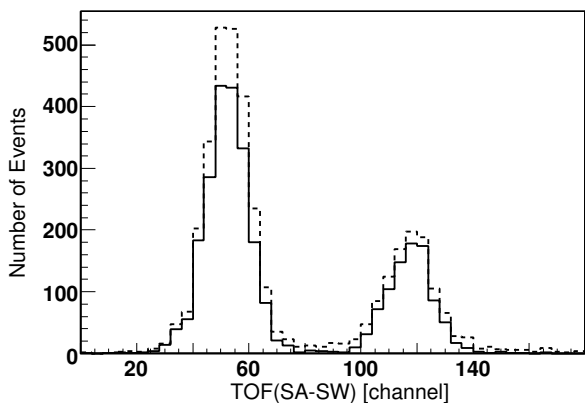
Fig. 1. The time-of-flight distributions of particles detected in one of the SA and one of the SW scintillators, obtained before (dashed) and after (solid line) the determination of their momenta. The reduced number of events in the latter case is the result of the efficiencies of the MWPCs and the track-finding algorithm. The bin width is equal to 4 channels. The left and right peaks arise, respectively, from pions and protons emitted from the target.
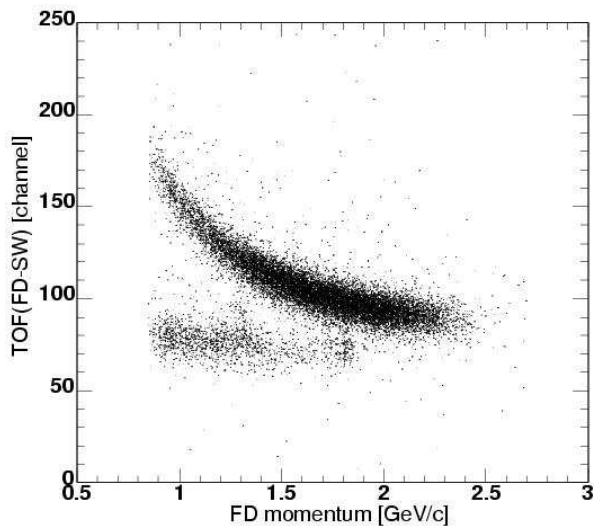
Fig. 2. The TOF difference between particles detected in the FD and protons in SW scintillators *versus* the momentum of particles in the FD. Protons detected in the FD produce the upper curved band whereas the TOF of pions is almost independent of the momentum.

found to decrease smoothly from 92% to 86% with increasing particle momentum and track inclination but to remain constant in the vertical direction for all SA-SW combinations involved in the later analysis.

In contrast to the PD, the two layers of scintillators used in the FD are placed very close to each other and, in order to identify protons, the TOF difference between the SW and FD scintillators had to be combined with the measurement of the momentum of particles detected in the FD, as shown in fig. 2. Coincident protons were selected in the PD as described above and their momenta reconstructed to make a correction for the different trajectory lengths. In the momentum range of interest,

which is below $1.8\,\mathrm{GeV}/c$, the proton and pion bands are well separated except in the vicinity of $1.75\,\mathrm{GeV}/c$. Here the numbers of pions are strongly enhanced by the proton-neutron final-state interaction in the $pp \to pn\pi^+$ reaction. However, if misidentified as protons, such pions will produce a peak in the pp missing-mass distribution at $0.65\,\mathrm{GeV}/c^2$ and $0.68\,\mathrm{GeV}/c^2$ for $2.85\,\mathrm{GeV}/c$ and $2.95\,\mathrm{GeV}/c$, respectively. This allows us the possibility to control the proton selection also in the overlap region of fig. 2. The total loss of protons as a result of the selection was estimated to be $(7 \pm 2)\%$.

To determine the efficiency of a single FD MWPC, the trajectory of a particle has been found using only information from the other two MWPCs. Having calculated the point at which the trajectory intersects the sensitive plane of the MWPC under investigation, the presence of a valid neighbouring cluster has been checked to satisfy all requirements applied in the track-finding algorithm [13]. This procedure resulted in an efficiency map for each of the sensitive planes, which was subsequently used to introduce the efficiency correction on an event-by-event basis. Only one sensitive plane among the seven involved in the FD track reconstruction was found to have an inhomogeneous distribution of efficiency in approximately 30% of its sensitive area, with an average value of 88%. All the others had homogeneous maps with average efficiencies between 96% and 99%.

In order to decrease both the statistical and systematic uncertainties in the efficiency corrections, cells with low statistics were excluded from the maps. A statistical accuracy of about 0.1% was then achieved. The systematic uncertainty was investigated using the deviations of the luminosity calculated in five angular bins from the average value. Having observed that the inhomogeneity of the efficiency in one MWPC was significantly different for the three different periods of data-taking, individual efficiency maps were produced for each of these periods. The pp elastic scattering contributed not more than 20% to the total statistics involved in the production of the maps. Luminosities were determined separately for each of these three time periods using the corresponding efficiency maps. The statistical errors were 0.7–1.1% per angular bin and all 15 values (5 angular bins × 3 time periods) fell within ±3% of the mean, with an RMS of about 1.3%. The result, integrated over the total time of the experiment, was quoted above.

The influence of the total efficiency corrections on the missing-mass distributions has been checked using the ratio of corrected to uncorrected spectra, which was found to be constant to within experimental errors. The average efficiency was about 75%.

3 Selection of pp → ppω events

Histograms representing the overall missing-mass (m_X) distributions from the $pp \to ppX$ reaction at the two beam momenta are shown in fig. 3.

Both spectra show similar features. There is a sharp rise from the kinematic limit on the right due to the mul-
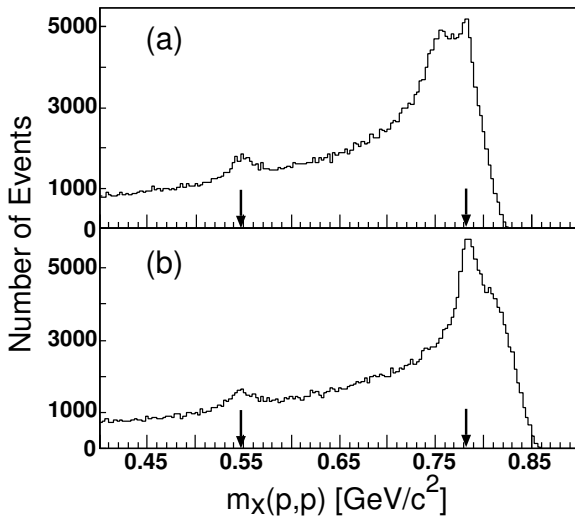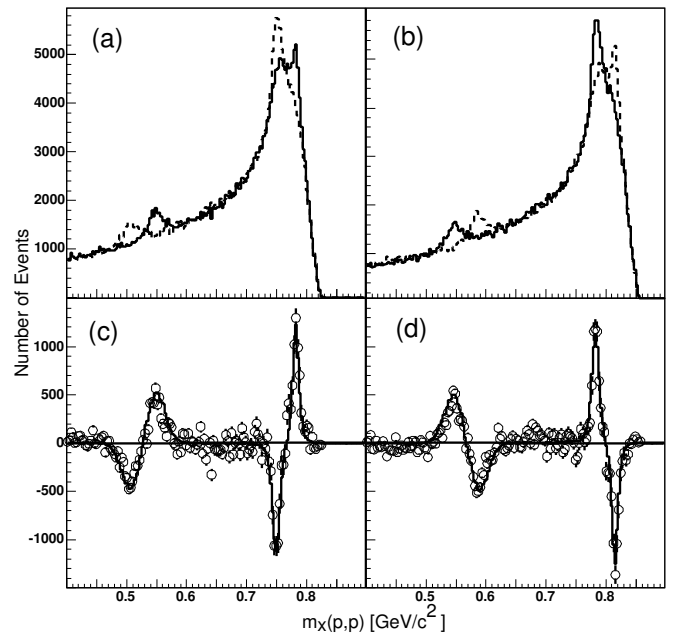
Fig. 3. The missing-mass distributions of the $pp \to ppX$ reaction in bins of $3 \, \text{MeV}/c^2$ measured (a) at $2.85 \, \text{GeV}/c$ and (b) at $2.95 \, \text{GeV}/c$. There is clear evidence for peaks corresponding to the production of both η and ω (indicated by arrows) but sitting on a large background.

Table 1. Missing masses of various reactions in MeV/c^2 for the two beam momenta.

m_X	$2.85 \, \text{GeV}/c$	$2.95 \, \text{GeV}/c$
$m_n(\pi^+_{PD}, p_{FD})$	939.3 ± 0.1	939.6 ± 0.1
$m_n(p_{PD}, \pi^+_{FD})$	939.2 ± 0.2	939.8 ± 0.2
$m_\eta(p_{PD}, p_{FD})$	547.8 ± 0.1	547.4 ± 0.1
$m_\omega(p_{PD}, p_{FD})$	782.3 ± 0.4	782.7 ± 0.4

tiparticle phase space, whereas the more gentle fall to the left is mainly a reflection of the ANKE acceptance. Sitting on top of this background there are small peaks due to the production of the η- and ω-mesons. Evidence for the $pp \to pp\pi^0$ reaction was also found below $0.4 \, \text{GeV}/c^2$, but the pion peak has a large width because the effects of momentum uncertainties are significantly amplified in this region of large excess energies.

The accuracy of the missing-mass reconstruction was verified using the $pp \to pp\eta$ and the $pp \to pn\pi^+$ reactions, with the results being presented in table 1. In the pion case, the neutron mass was reconstructed in both possible variants, either when the proton was found in the FD and the pion in the PD or *vice versa*. Given the good agreement achieved in these cases, one should expect to find the ω peak at its nominal position. However, in the vicinity of the ω mass, the large physical background, dominantly from multipion production, is strongly peaked, as shown in fig. 3. To select the ω signal, a kinematical transformation of the experimental missing-mass distribution from one beam momentum to the other was applied, as illustrated in fig. 4. This approach was proposed and successfully used in the study of ω production at lower excess energies with the SPESIII spectrometer [6]. It avoids the need to construct specific models for a background that is unlikely to follow phase space.

Fig. 4. The missing-mass distributions of the $pp \to ppX$ reaction in $3 \, \text{MeV}/c^2$ bins measured (a) at $2.85 \, \text{GeV}/c$, and (b) at $2.95 \, \text{GeV}/c$ are shown by solid lines. The dashed line in panel (a) represents the spectrum actually measured at $2.95 \, \text{GeV}/c$ but kinematically transformed to $2.85 \, \text{GeV}/c$, as described in the text. The dashed line in panel (b) shows the $2.85 \, \text{GeV}/c$ after transformation to $2.95 \, \text{GeV}/c$. The points in the lower frames (c) and (d) present the corresponding bin-by-bin differences of the two sets of distributions. The solid lines show simulations of the $pp \to pp\eta$ and $pp \to pp\omega$ reactions convoluted with acceptance. The widths of the peaks, which are strongly influenced by effects of momentum reconstruction, are very well reproduced.

The scheme involves an event-by-event Lorentz transformation of the momenta of both final protons from the laboratory system where they were actually measured to the laboratory system at another beam momentum. If the experimental acceptance covers only a small part of the phase space available for a background reaction, the shape of the corresponding missing-mass distribution is expected to be determined by the acceptance and to be almost completely insensitive to a change of the primary distribution over phase space. On the other hand, a peak corresponding to the production of a single meson is shifted by approximately the difference in centre-of-mass energies, as seen clearly for η production in figs. 4a,b. The solid histogram in fig. 4a shows the missing-mass distribution actually measured at $2.85 \, \text{GeV}/c$ (see also fig. 3a). The dashed histogram represents the result of such a transformation of the missing-mass distribution obtained at the $2.95 \, \text{GeV}/c$ beam momentum (see fig. 3b) to $2.85 \, \text{GeV}/c$. The transformed distribution is normalised by the ratio of the sums of events in the 0.6–$0.7 \, \text{GeV}/c^2$ range, which gives a factor of 1.054 ± 0.006. The inverse procedure involving the transformation from $2.85 \, \text{GeV}/c$ to $2.95 \, \text{GeV}/c$ leads to the results shown in fig. 4b.

The differences between the actual and transformed distributions, shown by points in figs. 4c,d, demonstrate

clear positive (negative) peaks corresponding to η and ω production in the actual (transformed) cases. These peaks are in a good agreement with the results of the phase space simulations of these reactions (solid line), where the η and ω experimental widths arise mainly from the uncertainties in the momentum reconstruction. The missing-mass distributions simulated at $2.95\,\mathrm{GeV}/c$ were first adjusted to the experimental data at that beam momentum before being transformed to $2.85\,\mathrm{GeV}/c$ and subtracted in the same way as for the experimental points, and *vice versa.* Finally, the difference spectra for $m_X > 0.65\,\mathrm{MeV}/c^2$ in figs. 4c (d) were fitted by two Gaussian functions in order to extract the number of events in the ω peak, its statistical uncertainty, and the position of the peak at $Q = 60\,\mathrm{MeV}$ ($92\,\mathrm{MeV}$) (see table 1).

The comparison of the numbers obtained from the fits at both energies, as well as the results of simulations, shows that, in this particular case, after taking into account the normalisation factor, the number of ω-mesons produced at $2.95\,\mathrm{GeV}/c$ could also be extracted from the negative peak in fig. 4c. Nevertheless, we would like to emphasise that, away from the kinematic limit, the transformation is not a trivial shift of the missing-mass distribution by the difference of centre-of-mass energies. It is not possible *a priori* to decide from which masses the transformation starts to change the shape of distribution and so the approach should not be considered as a universal method that can automatically be applied under any experimental conditions. Moreover, the good agreement found for the shapes of the background spectra in the region between the η and ω peaks does not necessarily prove that the same is true also underneath the ω peaks. In principle, up to six pions might be produced at our energies, but only those with two and three pions in the final state have phase spaces much larger than the ANKE acceptance. Although the total cross-sections for the production of four or more pions are at least an order of magnitude smaller, they have larger acceptances in ANKE and populate missing masses mostly near the kinematical limit, as would also the products of the $pp \rightarrow K^+\Lambda p$ reaction, where Λ decays into $p\pi^-$.

The direct way of verifying the shape of the background under the ω peak, by interpolating between two transformed distributions measured above and below the given excess energy, is not possible here since the data were taken at only two energies. An attempt to describe the multipion background with the help of phase space simulations, adjusting the relative contribution of reactions with different number of pions, was also undertaken. However, no set of parameters could simultaneously provide an appropriate reproduction of the background shape in different parts of the acceptance, probably due to the neglect of all resonance effects. We have therefore used the following procedure to evaluate the possible variation in the shape near the kinematical limit in the missing mass.

Since the shape of the background varies across the total spectrometer acceptance, an acceptance range was found where the shape could be directly established from the fit procedure. The results from this are shown in fig. 5.
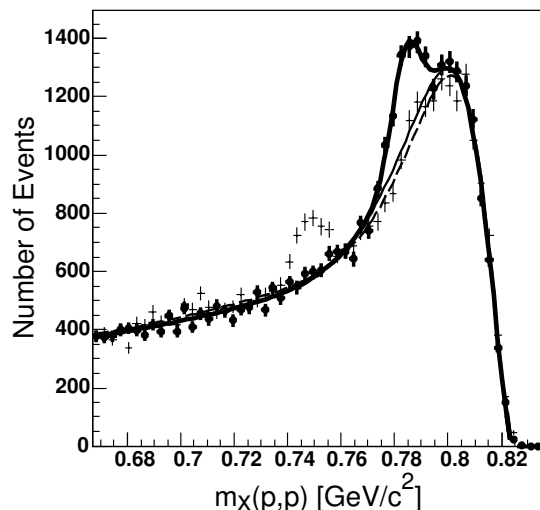
Fig. 5. The missing-mass distribution of the $pp \rightarrow ppX$ reaction in bins of $3\,\mathrm{MeV}/c^2$ obtained at $2.85\,\mathrm{GeV}/c$ within a restricted part of the total acceptance (closed circles) is shown together with the corresponding distribution kinematically transformed from $2.95\,\mathrm{GeV}/c$ to $2.85\,\mathrm{GeV}/c$ (crosses). The thick solid line represents a fit to the distribution at $2.85\,\mathrm{GeV}/c$, while the thin one shows the background function under the ω peak found in this case. The same fit procedure was applied to the transformed distribution and the resulting background function shown by the dashed line.

Both the measured and the transformed distributions were then separately fitted, using the same function to describe the background, together with a Gaussian function for the ω peak. The transformed distribution in fig. 5 was scaled by 1.086 ± 0.011, *i.e.* the ratio of the integrals under the background functions obtained in this way. The ratio of the background functions is not quite constant over the range but, apart from the 5–$7\,\mathrm{MeV}/c^2$ interval next to the kinematical limit, the deviation from unity is rather small. The difference between the background functions observed near the maximum of the distribution does not exceed 5%, changing sign in the vicinity of $0.75\,\mathrm{GeV}/c^2$, and staying at the 2% level at smaller masses. Since the accuracy of the fit is similar to these deviations, a variation of 3% has been considered as a measure of the systematics when the number of events under the ω peak could be determined only from the difference of experimental distributions at different energies.

The total numbers of ω-mesons deduced from fits to the distribution at $2.85\,\mathrm{GeV}/c$ shown in the lower frame of fig. 4, and the analogous one at $2.95\,\mathrm{GeV}/c$, were found to be

$$5560 \pm 540(\mathrm{stat.}) \pm 660(\mathrm{syst.}) \text{ at } Q = 60\,\mathrm{MeV},$$
$$5360 \pm 480(\mathrm{stat.}) \pm 720(\mathrm{syst.}) \text{ at } Q = 92\,\mathrm{MeV}.$$

The large statistical errors are the result of the subtraction procedure as well as the need to describe two peaks of opposite sign situated close to each other.

4 Analysis of differential distributions

The restriction on the particle momenta registered in the PD leads to some mismatch in the FD and the PD mo-

mentum ranges and this in turn results in a limitation on the $pp \rightarrow pp\omega$ phase space available within the ANKE acceptance. The acceptance corrections can therefore not be done in a model-independent way and some assumptions have to be made on the differential distributions to determine the total cross-section. To test the validity of the assumptions discussed below, we have compared a number of one-dimensional $pp \rightarrow pp\omega$ experimental distributions with the results of simulations. The following observables have been considered:

- The kinetic energy of the final pp pair in their rest frame: $\varepsilon_{pp} = M_{\mathrm{inv}}(p,p) - 2m_p$, where $M_{\mathrm{inv}}(p,p)$ is the pp invariant mass.
- The kinetic energy of the ω-meson and the proton detected in the PD in their rest frame: $\varepsilon_{\omega p} = M_{\mathrm{inv}}(\omega,p) - m_p - m_\omega$. In this case, the full range of the ωp invariant masses $M_{\mathrm{inv}}(\omega,p)$ could be covered due to the large FD momentum acceptance. However, when the proton was detected in the FD, the range of $\varepsilon_{\omega p}$ was less than 40 MeV and 75 MeV at excess energies of 60 MeV and 92 MeV, respectively.
- The angle of the ω-meson with respect to the beam direction in the overall centre-of-mass system: $\cos\Theta_{\mathrm{cm}}$.
- The angle of a proton momentum $\boldsymbol{q}$ with respect to the beam direction in the rest frame of the final pp pair: $\cos\Theta_{pp}$.
- The angle of $\boldsymbol{q}$ with respect to the momentum of the ω-meson in the rest frame of the final pp pair: $\cos\Psi_{pp}$.

The number of ω-mesons in each bin of such a distribution was determined from the corresponding missing-mass spectrum using approaches that depended slightly on the shape of the background and the position of the ω peak relative to the upper edge of the spectrum.

- When, as in fig. 5, the shape of the background could be clearly established, a preference was given to the fit procedure described above. The missing-mass transformation was used to check that the description of the background below the ω peaks was reasonable. It was found that the normalisation factor of the transformed missing-mass distribution to the measured one is not constant, but may vary by up to 7%. Therefore, this factor had to be determined for each bin.
- In cases where the fit procedure could only be applied at a single excess energy, generally at 92 MeV, the background function for the corresponding transformed distribution was obtained. A simple scaling of this function was then allowed which, together with a Gaussian ω peak, was used to fit the distribution measured at the other excess energy. The scaling parameter thus obtained was used for the normalisation of the transformed distribution to the measured one. The number of ω-mesons obtained as a result of the fit was verified using the difference of distributions of the type shown in fig. 4. This procedure was also applied at $\varepsilon_{pp} > 60$ MeV, where the distributions transformed from 2.85 GeV/c to 2.95 GeV/c no longer contained the ω peak.
- The scenarios outlined above describe more than 80% of our data. For the remainder, the transformed dis-
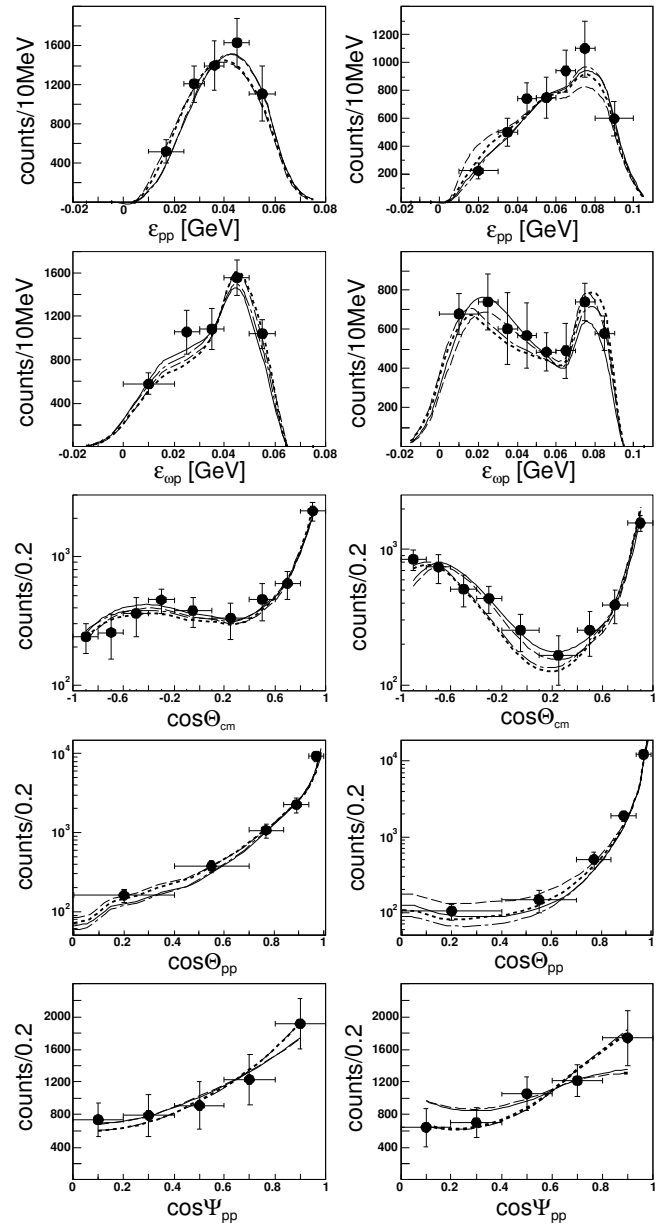
Fig. 6. The distributions of experimental (points) and simulated (lines) ω-meson yields for different reaction observables at 60 MeV (left panels) and 92 MeV (right panels). The different simulations correspond to pure phase space PS (solid line), full FSI (dashed line), phase space distorted by an angular dependence in the Ψ_{pp} variable (dash-dotted line), and partial FSI with the distorted angular distribution (dotted line), as described in the text. The corresponding total cross-sections are given in table 2.

tribution was normalised by the ratio of the numbers determined after excluding the range covered by the actual and the transformed ω peaks from each of the spectra. It was verified that the sum of background events under the actual ω peak found in this and the previous two cases is equal within errors to the total number of background events shown in fig. 4.

In all the cases, different assumptions regarding the background functions and/or different normalisation factors were tested in order to establish possible systematic errors, and these are incorporated into the vertical error bars on the points presented in fig. 6.

The $pp \rightarrow pp\omega$ reaction was simulated at both excess energies using the PLUTO event generator [14] under different assumptions on the distribution of events over the total phase space of the reaction. Both protons were traced through the ANKE acceptance with the help of the GEANT3 package [15]. To check the tracing procedure, the momentum and angular acceptances of all the scintillators, as well as their images in the MWPCs, have been evaluated and compared with the corresponding experimental ones. They were found to coincide to within the experimental errors. Finally, the total number of accepted events simulated at each excess energy was normalised to the corresponding total number of ω-mesons obtained in the experiment.

The solid lines in fig. 6 demonstrate the distributions expected in the case of a three-body phase space (PS), whereas those shown by dashed lines take into account the final-state interaction (FSI) between the two protons. Following Goldberger and Watson [16], the FSI enhancement factor $I(q)$ was calculated using the Jost function $J(q)$:

$$I(q) = |J(q)|^{-2} = \left(\frac{q^2 + \beta^2}{q^2 + \alpha^2} \right), \qquad (4.1)$$

where $q = |\boldsymbol{q}|$ is the magnitude of the proton momentum in the pp rest frame. On the basis of the pp scattering length and effective range, we took $\alpha = -20.5\,\mathrm{MeV}/c$, $\beta = 167\,\mathrm{MeV}/c$.

Due to the selection of one proton in the FD and the other in the PD, the experiment had no acceptance for $\varepsilon_{pp} < 10\,\mathrm{MeV}$. As a consequence, and as shown by the left panels of fig. 6, the distributions at $Q = 60\,\mathrm{MeV}$ cannot distinguish between the pure PS and FSI models. However, at $Q = 92\,\mathrm{MeV}$, the experimental yield in the $10 < \varepsilon_{pp} < 30\,\mathrm{MeV}$ range is about a factor of two lower than that expected on the basis of the FSI model. It must be noted that the yield in this bin can be determined very reliably, as shown by the corresponding missing-mass spectrum in fig. 7. The fit procedure applied to the missing-mass distribution at $Q = 92\,\mathrm{MeV}$ would give an even smaller yield than that found taking into account the behavior of the transformed spectrum under the peak. Different background functions were tested, but none of them could increase the yield by more than 25% assuming a smooth shape under the ω peak.

The low experimental yield at $Q = 92\,\mathrm{MeV}$ for $\varepsilon_{pp} < 30\,\mathrm{MeV}$ is similar to that observed in the analogous $pp \rightarrow pp\eta$ reaction at 74 MeV, where the effects of the FSI in the pp system were found to be very small [17]. This may be an indication that the pp S-wave is weak and that higher pp partial waves are important. In this connection it should be noted that the distributions in the proton angles in the pp rest frame, especially Ψ_{pp}, would allow some anisotropy. The dash-dotted lines in fig. 6 were calculated assuming
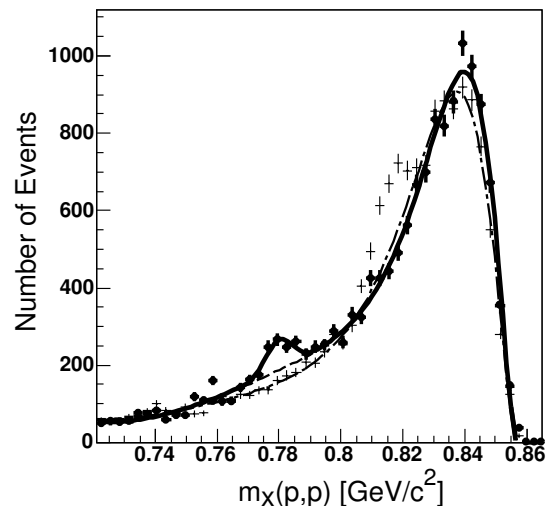
Fig. 7. Missing-mass distribution of the $pp \rightarrow ppX$ reactions in bins of $4\,\mathrm{MeV}/c^2$ obtained at $Q = 92\,\mathrm{MeV}$ in the $10 < \varepsilon_{pp} < 30\,\mathrm{MeV}$ range (closed circles) is shown together with the corresponding transformed distribution (crosses). The thick solid line represents the fit result for the measured spectrum. The dashed and dash-dotted lines show two extreme cases of the background behaviour. The maximum systematic error was established to be 25%.

Table 2. Total cross-sections for different models. The form of the FSI factor is given in eq. (4.1) and that of the assumed angular dependence in eq. (4.2).

	$Q = 60\,\mathrm{MeV}$	$Q = 92\,\mathrm{MeV}$
Model	$a = 0.2$	$a = 0.6$
	$k = 0.8$	$k = 0.4$
PS	$5.0\,\mu\mathrm{b}$	$10.8\,\mu\mathrm{b}$
PS + FSI(100%)	$7.1\,\mu\mathrm{b}$	$14.3\,\mu\mathrm{b}$
PS + $a\,P_2(\cos\Psi_{pp})$	$4.8\,\mu\mathrm{b}$	$10.4\,\mu\mathrm{b}$
PS + $k \times$ FSI + $a\,P_2(\cos\Psi_{pp})$	$6.6\,\mu\mathrm{b}$	$12.0\,\mu\mathrm{b}$

that the three-body phase space is modified by a factor

$$1 + a\,P_2(\cos\Psi_{pp}), \qquad (4.2)$$

where $P_2(\cos\Psi_{pp})$ is a Legendre polynomial, and $a = 0.6$ at $Q = 92\,\mathrm{MeV}$. At $Q = 60\,\mathrm{MeV}$ we would expect any anisotropy to be smaller. The case of $a = 0.2$ was tested but, for all the observables other than $\cos\Psi_{pp}$, the results differ little from the PS case.

Although the introduction of an angular dependence through eq. (4.2) provides a quite adequate description of all the distributions, with no need for the S-wave FSI, it seems unlikely that this would be suppressed completely. To test some of the possibilities, we have adjusted the contribution of the FSI to provide a slightly better description of the data; the results shown by dotted lines in fig. 6 were achieved by decreasing the FSI enhancement by factors of 0.8 and 0.4 at $Q = 60\,\mathrm{MeV}$ and 92 MeV, respectively. The values of the total cross-sections obtained on the basis of these various assumptions are presented in table 2.

It is interesting to note that at $Q = 92\,\mathrm{MeV}$ the introduction of an anisotropic distribution in the Ψ_{pp} angle improves also the description of data in the Θ_{cm} angle in the region of $\cos\Theta_{\mathrm{cm}} = -0.9$. This was the only way that was found to ensure the required symmetry in this variable about $\Theta_{\mathrm{cm}} = 90°$. In contrast to the Ψ_{pp}-dependence, the distribution in the meson centre-of-mass angle seems to be rather flat at both the excess energies. Nevertheless, the effects of a possible Θ_{cm} anisotropy on the evaluation of the total cross-section have also been investigated, assuming a variation analogous to that in eq. (4.2). It was found that values of a lying between -0.15 and $+0.3$ gave an acceptable description of the whole set of data at both the excess energies, comparable to that shown in fig. 6 by dotted lines, while larger anisotropies are unfavoured. In their preliminary results, the COSY-TOF Collaboration reported even smaller values of the anisotropy parameter a at $Q = 92\,\mathrm{MeV}$ [18]. For such small values of a, any changes that it induces in the total cross-section fall within the ranges presented in table 2.

As seen from fig. 6, there is a sharp forward-backward peaking of the experimental acceptance over the Θ_{pp} angle so that even a small anisotropy here would lead to a large change in the total cross-section. However, this distribution is strongly correlated with the yield at low ε_{pp} and this significantly restricts any possible variation arising from the anisotropy. In order to provide a reasonable description of the data, any dependence on Θ_{pp} has to be compensated by changing the FSI contribution. Since these two effects change the acceptance corrections in opposite directions, the variation of the total cross-section values still does not fall outside the ranges in the table.

5 Results and discussion

Combining the results of all the variants that can hardly be distinguished within the errors, we find total cross-sections lying in the ranges 4.8–$7.1\,\mu\mathrm{b}$ at $Q = 60\,\mathrm{MeV}$ and 10.4–$14.3\,\mu\mathrm{b}$ at $92\,\mathrm{MeV}$, respectively. The highest values are achieved with the rather unrealistic pure FSI model and so we take rather the last two lines of table 2 as an indication of the model dependence of the results. These give

$$\sigma(Q = 60\,\mathrm{MeV}) = (5.7 \pm 0.6_{\mathrm{stat}} \pm 0.8_{\mathrm{syst}} \pm 0.9_{\mathrm{mod}})\,\mu\mathrm{b},$$
$$\sigma(Q = 92\,\mathrm{MeV}) = (11.2 \pm 1.1_{\mathrm{stat}} \pm 1.7_{\mathrm{syst}} \pm 0.8_{\mathrm{mod}})\,\mu\mathrm{b},$$

where the first error represents the statistical uncertainty. The second figure stands for the total experimental systematic uncertainty, which includes contributions from the luminosity determination, the possible change of acceptance due to uncertainties in the detector positioning, but mainly the determination of the total number of $pp\omega$ events. These were all treated as independent errors. The final number is our estimate of the influence of the model on the acceptance calculation.

Our $pp \to pp\omega$ total cross-sections are shown in fig. 8 with vertical error bars estimated from the quadratic sum of both the systematic and statistical errors presented above. Also shown are the results of other experiments at
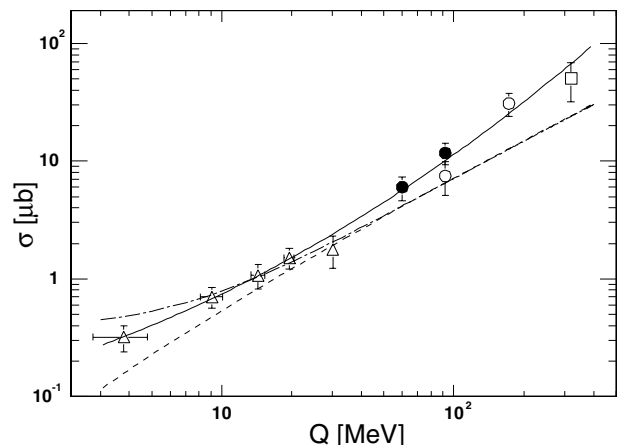
Fig. 8. The energy dependence of the $pp \to pp\omega$ total cross-section. Our two points (closed circles) are compared with earlier data from refs. [6] (triangles), [7] (square), and [8] (open circles). In all cases, systematic and statistical errors have been added in quadrature. The chain and dashed curves show respectively the normalised energy dependence of eq. (5.2) with and without smearing over the finite ω width. The solid line is a purely phenomenological interpolation of the whole data set given by eq. (5.1).

low Q [6–8]. The $92\,\mathrm{MeV}$ value is slightly higher than that of TOF, though the error bars do overlap. With the possible exception of the highest SPESIII point, the results are consistent with a smooth energy dependence and a global fit to the whole data set yields

$$\log_{10}\sigma = -0.855 + 0.495\log_{10}Q + 0.230\left(\log_{10}Q\right)^2, \quad (5.1)$$

where Q is measured in MeV and the cross-section in $\mu\mathrm{b}$. This is also shown in the figure.

In the SPESIII work [6], the energy dependence of the total cross-section was compared with a simplistic model, consisting only of three-body phase space but modified by the S-wave pp FSI [19]. This leads to the analytic result

$$\sigma(pp \to pp\omega) = C_\omega \left(\frac{Q/\epsilon}{1 + \sqrt{1 + Q/\epsilon}}\right)^2, \quad (5.2)$$

where $\epsilon \approx 0.45\,\mathrm{MeV}$. However, at low excess energies it is important to smear this function over the width of the ω-meson. Both these forms are shown in fig. 8, with the value of $C_\omega = 37\,\mathrm{nb}$ being chosen to fit the SPESIII points rather than those at higher energy. Although the S-wave assumption is clearly untenable at larger Q, the curves do suggest that P or higher partial waves are important there and a good representation of the data can be obtained by adding a small amount of pure phase space distribution to the FSI of eq. (5.2). While presenting a baseline against which one can judge the more refined theoretical models, this approach also shows that the finite-width effects are negligible in our energy domain.

The predictions of three microscopic models [3–5] are shown in fig. 9. All of them are versions of a meson exchange model, but with different emphasis on the role of
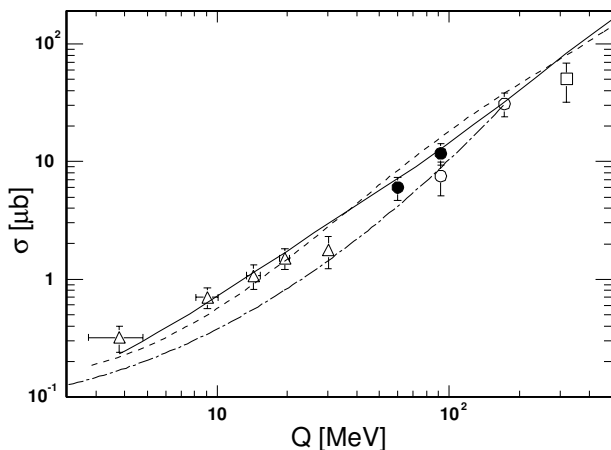
Fig. 9. Experimental data on the $pp \to pp\omega$ total cross-section shown in fig. 8 compared with the predictions from microscopic theoretical models shown by the chain [3], solid [4], and dashed [5] curves.

the N^* isobars. It should be noted that these calculations involve a large number of parameters, some of which have been adjusted in order to optimise the agreement with the published data, including the differential distribution at 173 MeV [8].

In the early work of Tsushima and Nakayama [3], nucleonic and mesonic current contributions were considered but the energy dependence of the total cross-section is described better by the inclusion of effects of nucleon resonances, and it is that curve which is shown in fig. 9. Nevertheless, this calculation still underestimates the SPESIII data by about a factor of two even though the finite ω width was taken into account. Despite neglecting this, and the initial-state interaction, Kaptari and Kämpfer [4] got good agreement with the then available data without relying on any N^* contribution. It was shown there that the effects of the S-wave FSI are particularly important, for without it a phase space energy dependence of the Q^2 type is predicted. The Tübingen group [5] had extensive recourse to several nucleon resonances, especially to the $N^*(1535)$, but the novel feature of their approach is the coupling to off-shell ω-mesons, which is particularly important close to the reaction threshold. If this is correct, then one would expect interesting effects when ω is measured exclusively through its e^+e^- decay mode [5].

Having new information on the energy dependence of the $pp \to pp\omega$ total cross-section, we can investigate further the ratio of ϕ to ω production near threshold within the context of the OZI rule [2]. If the (ω, ϕ) mixing in the vector meson nonet were ideal, such that ϕ were a pure $s\bar{s}$ state, then its three-pion decay would be forbidden by the OZI rule. That it takes place at all is interpreted as an indication that the mixing is not quite ideal. Using the Gell-Mann–Okubo mass formulae, Lipkin [20] estimated that the ratio of coupling strengths of ϕ and ω to nonstrange hadrons should be

$$R_{\text{OZI}} = 4.2 \times 10^{-3}. \tag{5.3}$$

It is therefore useful to evaluate the ratio of the ϕ and ω production cross-sections in *pp* collisions at the same value of the excess energy:

$$R_{\phi/\omega} \equiv \frac{\sigma(pp \to pp\phi)}{\sigma(pp \to pp\omega)}. \tag{5.4}$$

Taking the recent measurement [9] of the total cross-section for ϕ production in *pp* collisions at $Q = 18.5$, 34.5, and 75.9 MeV in conjunction with the global fit of eq. (5.1) to the data set of fig. 8, we find at these energies $R_{\phi/\omega} = (3.1 \pm 0.6) \times 10^{-2}$, $(3.0 \pm 0.7) \times 10^{-2}$, and $(2.4 \pm 0.7) \times 10^{-2}$, respectively, where all error bars have been compounded quadratically. Applying the same procedure to the ϕ point reported by the DISTO Collaboration leads to $R_{\phi/\omega} = (2.2 \pm 1.0) \times 10^{-2}$ at 83 MeV. The mean value of $R_{\phi/\omega} = (2.8 \pm 0.4) \times 10^{-2} \approx 7 \times R_{\text{OZI}}$, is lower than that obtained in ref. [9] because of the higher values for ω production that are now apparent in fig. 8. Although not statistically significant, there are indications from these numbers that $R_{\phi/\omega}$ might decrease with rising Q but, to test this, data would be needed on ϕ production at higher values of Q. However, it should be noted that such a slow decline had been predicted in model calculations. This arises there through the decreasing effect of the destructive interference between the nucleonic and mesonic contributions to ω production as the energy is raised [21]. There are, of course, other mechanisms proposed to explain such violations of the OZI rule as seen, for example, in refs. [3–5, 22] and references therein.

6 Conclusions

We have presented new measurements of the $pp \to pp\omega$ reaction at excess energies of 60 and 92 MeV. The SPESIII technique [6] of kinematically shifting the data at one energy to estimate the background at a neighbouring energy was successfully employed for differential as well as total spectra. In this way the small ω signal in the missing-mass distribution could be identified despite the large amount of multipion production. With the setup actually employed for studying this reaction at ANKE, the acceptance, especially at small ε_{pp}, was limited. A variety of assumptions were tested against one-dimensional spectra in order to assess the model dependence of the total ω production cross-section that we obtained in this way. This led to uncertainties that were comparable to the statistical and other systematic errors. The value for the total cross-section at 92 MeV is a little higher than that found by the TOF group [8], but our two points join smoothly with the results of other experiments. There is evidence from the anisotropic *pp* angular distribution at 92 MeV that P or higher *pp* partial waves are significant at this energy.

The new data allow us to extract the OZI ratio with greater confidence and smaller error bars than before. This results in a slightly smaller value of $R_{\phi/\omega}$ than previously quoted [9], with possibly a hint of some energy dependence [23].

All three theoretical calculations considered [3–5] appeared after the broad outlines of the energy dependence of the total cross-section had been determined experimentally and in some cases the model parameters were adjusted to reproduce this. Other experimental observables such as differential cross-sections or decay angular distributions are needed to constrain the models more tightly and it is encouraging to note that analysing power results will soon be made available by the COSY-TOF Collaboration [24]. Since good data exist on $pn \to d\phi$ at low energies [25], further data on ω production with a neutron target would be particularly helpful [26].

The WASA at COSY facility will soon become operational [27]. The production of ω in pp collisions could then be investigated, with larger geometrical acceptance and lower background, *via* the detection of the $\omega \to \pi^0\gamma$ decay ($BR \approx 9\%$) and the reconstruction of its invariant mass. Such an approach would also have the advantage of leading to a determination of the tensor polarisation of ω, a quantity which is very sensitive to the presence of higher partial waves. A similar sensitivity also exists in the spin-spin correlation in $\vec{p}\,\vec{p} \to pp\omega$, which could be measured at ANKE [28].

References

1. C. Hanhart, Phys. Rep. **397**, 155 (2004).
2. S. Okubo, Phys. Lett. **5**, 165 (1963); G. Zweig, CERN report TH-401 (1964); J. Iizuka, Prog. Theor. Phys. Suppl. **38**, 21 (1966).
3. K. Tsushima, K. Nakayama, Phys. Rev. C **68**, 034612 (2003).
4. L. P. Kaptari, B. Kämpfer, Eur. Phys. J. A **23**, 291 (2005).
5. C. Fuchs *et al.*, Phys. Rev. C **67**, 025202 (2003).
6. F. Hibou *et al.*, Phys. Rev. Lett. **83**, 492 (1999).
7. F. Balestra *et al.*, Phys. Rev. C **63**, 024004 (2001).
8. S. Abd El-Samad *et al.*, Phys. Lett. B **522**, 16 (2001).
9. M. Hartmann *et al.*, Phys. Rev. Lett. **96**, 242301 (2006).
10. S. Barsov *et al.*, Nucl. Instrum. Methods A **462**, 364 (2001).
11. A. Khoukaz *et al.*, Eur. Phys. J. D **5**, 275 (1999).
12. R.A. Arndt *et al.*, Phys. Rev. C **62**, 034005 (2000); solution SP05 (0–3 GeV) from http://gwdac.phys.gwu.edu.
13. S. Dymov *et al.*, Part. Nucl. Lett. **2**, 40 (2004).
14. Pluto WEB page: http://www-hades.gsi.de/computing/pluto/html/PlutoIndex.html.
15. GEANT3, CERN Program Library W5013, CERN, 1993; http://wwwinfo.cern.asdoc/geant_html3/geantall.html.
16. M.L. Goldberger, K.M. Watson, *Collision Theory* (John Wiley & Sons, New York, 1964) p. 549.
17. C. Pauly, PhD Thesis, University of Hamburg (2006).
18. M. Schulte-Wissermann, PhD Thesis, University of Dresden (2004).
19. G. Fäldt, C. Wilkin, Phys. Lett. B **382**, 209 (1996).
20. H.J. Lipkin, Phys. Lett. B **60**, 371 (1976).
21. K. Nakayama, J. Haidenbauer, J. Speth, Phys. Rev. C **63**, 015201 (2000).
22. A. Sibirtsev, J. Haidenbauer, U.-G. Meißner, Eur. Phys. J. A **27**, 263 (2006).
23. V. Blobel *et al.*, Phys. Lett. B **59**, 88 (1975); R. Baldi *et al.*, Phys. Lett. B **68**, 381 (1975).
24. K. Brinkmann (private communication).
25. Y. Maeda *et al.*, Phys. Rev. Lett. **97**, 142301 (2006)
26. S. Barsov *et al.*, Eur. Phys. J. A **21**, 521 (2004).
27. B. Höistad, J. Ritman (Editors) *WASA at COSY*, COSY proposal, arXiv:nucl-ex/0411038.
28. A. Kacharava, F. Rathmann, C. Wilkin, *Spin Physics from COSY to FAIR*, COSY proposal no. 152 (2005) arXiv:nucl-ex/0511028.